



PCCP

A Hybrid Theoretical Method for Predicting Electrokinetic Energy Conversion in Nanochannels

Journal:	<i>Physical Chemistry Chemical Physics</i>
Manuscript ID	CP-ART-02-2020-000997.R1
Article Type:	Paper
Date Submitted by the Author:	21-Mar-2020
Complete List of Authors:	Hu, Xiaoyu; Chemical Engineering, Chemical Engineering Nan, Yiling; University of Alberta Kong, Xian; Institute of Biochemical Engineering, Chemical Engineering; Lu, Diannan; Chemical Engineering, Chemical Engineering Wu, Jianzhong; University of California, Riverside, Chemical and Environmental Engineering

SCHOLARONE™
Manuscripts

A Hybrid Theoretical Method for Predicting Electrokinetic Energy Conversion in Nanochannels

Xiaoyu Hu^{a)}, Yiling Nan^{a),c)}, Xian Kong^{a)}, Diannan Lu^{a)}, Jianzhong Wu^{b)}

^{a)}*Department of Chemical Engineering, Tsinghua University, Beijing 100084, China*

^{b)}*Department of Chemical and Environmental Engineering, University of California, Riverside, California 92521, United States*

^{c)}*School of Mining and Petroleum Engineering, Department of Civil and Environmental Engineering, University of Alberta, Edmonton, AB T6G 1H9, Canada*

Abstract

The traditional methods to predict electrokinetic energy conversion (EKEC) in nanochannels are mostly based on the Navier-Stokes (NS) equation for ionic flow and the Poisson-Boltzmann (PB) equation for charge distributions, which is questionable for ion transport through highly charged nanochannels. In this work, the classical density functional theory (cDFT) is used together with molecular dynamics (MD) simulation and the Navier-Stokes (NS) equation to predict the electrical current and thermodynamic efficiency of electrokinetic energy conversion in nanochannels. By introducing numerical results for the slip length calculated from MD simulation, a significant increase of the electrokinetic current is predicted in comparison to that from the traditional electrokinetic equations with the non-slip boundary condition, leading to the theoretical predictions of the thermodynamic efficiency for electrokinetic energy conversion in nanochannels in good agreement with recent experiments. The hybrid method predicts that a maximum electrokinetic efficiency can be achieved by tuning

^{a)} Electronic mail: ludiannan@tsinghua.edu.cn

^{b)} Electronic mail: jwu@enr.ucr.edu

the channel height and solution conditions including electrolyte concentrations, ion valences, and surface energies. The theoretical results provide new insights into pressure-driven electrical energy generation processes and helpful guidelines for engineering design and optimization of electrokinetic energy conversion.

I. INTRODUCTION

Electrical power can be produced by a pressure-driven process with an electrolyte solution flowing through charged nanochannels.¹⁻³ The so-called electrokinetic energy conversion (EKEC) plays a vital role in renewable energy generation and storage.^{1, 4} Thanks to rapid and steady improvement in nano-manufacturing capability, significant progress has been made in recent years on the EKEC technology,⁵⁻¹³ and it represents one of the most promising processes to achieve efficient conversion of hydraulic power to electricity.¹⁴ Compared with electromagnetic power generators, EKEC has one major advantage because it avoids macroscopic mechanical motions.⁴

Pioneering studies of EKEC processes were reported by Osterle and co-workers¹ and by Burgreen and Nakache for ultrafine capillaries.¹⁵ The early theoretical studies predicted that the maximum thermodynamic efficiency was only about 17 %, which is unattractive for many practical applications. A larger efficiency could be achieved by introducing buffer ions⁵. Gillespie investigated the effect of layering ions on the electrokinetic conversion theoretically and predicted that the maximum thermodynamic efficiency can be significantly increased up to 50%.¹⁶ More recent modelling of EKEC processes also indicates that the maximum thermodynamic efficiency can reach up to 30-40%, or as high as 50 % when the hydrodynamic slip and ion layering were explicitly considered.^{11, 13}

Experimental investigation of EKEC processes based on micro-channel arrays showed disappointing thermodynamic efficiency, merely $\sim 1\%$.^{17, 18} With the help of nano-manufacture technology, a higher efficiency can be obtained in nanochannels. More recently, an efficiency of 35%-46% was reported for ion transport through nitrocellulose/sulfonated polystyrene membranes.^{19, 20} A ballistic electrostatic generator may lead to an efficiency of 50%²¹. Some researchers utilized the method of measurement of the electrokinetic figure-of-merit, which is the gold standard for assessing the thermoelectric energy conversion of the materials²² and the reported efficiency is about 14~18% for Nafion at room temperature.²³ The thermodynamic efficiency increases to 26% when the process is implemented at 343 K.²⁴

A more reliable prediction of EKEC performance will help to identify optimal operation conditions and reduce the cost of the device.²⁵ The traditional methods are mostly based on the Navier-Stokes (NS) equation for ionic flow and the Poisson-Boltzmann (PB) equation for charge distributions. Because the ions are treated as point charges and the electrostatic correlations are neglected, the theoretical performance is questionable for ion transport through highly charged (~ 100 mC/m²) nanochannels as reported in the recent literature.² Besides, the conventional methods fail to capture the boundary conditions underlying the electroosmotic flows near a highly charged surface.²⁶ In a previous work²⁶, we compared the PB equation and the classical density functional theory (cDFT) in detail and showed how the thermodynamic non-ideality due to ion-ion interactions influence the transport properties of ionic microfluidics. In comparison with molecular simulations, cDFT has the advantage of computational efficiency, making it an ideal tool to explore the optimal parameters. While the nonslip boundary condition is often assumed in conventional electrokinetic models, both experiments²⁷⁻²⁹ and molecular simulations^{30, 31} indicate significant deviation from the non-slip assumption for nanochannels. In

our previous work²⁶, the channel width was fixed at 58 nm in the theoretical model, the same as that used in experiment². In this work, the widths of nanochannels vary from 2 nm to 7 nm. According to experimental results³², the water flow in a 7 nm-diameter nanotube is about 3000 times larger than that in a 44 nm-diameter nanotube³³, and the enhancement factor of the water flow in a less than 2nm-diameter nanotube³⁴ is about 25~300 times larger than that in the 44-diameter nanotube³³. Under such conditions, the traditional Navier-Stokes equation is not able to account for the EKEC current and thermodynamic efficiency. By contrast, the present model captures the drastic increase of the water flow in nanochannels in good agreement with experiments.

By combing cDFT with the NS equation and MD simulation, we hope to attain a faithful description of the electrical current and thermodynamic efficiency for electrokinetic energy conversion in nanochannels thus providing helpful guidelines for practical applications.

II. MODEL AND METHODS

We consider pressure-driven ion transport through slit-like nanochannels similar to previous theoretical and experimental investigations. We choose this setup not only because of its simplicity for the theoretical analysis but also for its easy manufacturing and surface-controlled properties from the experimental perspective. In addition to its usage in energy conversion, slit-like nanochannels find applications in many other fields, such as energy recovery, desalination, and single molecule detection.³⁵⁻³⁸

As shown schematically in **Fig. 1(a)**, both the ion distribution and solvent velocity are highly inhomogeneous near the charged surface as an electrolyte flows through a voltage-gated slit nanochannel driven by a pressure gradient. To describe the ion distribution (*viz.*, the structure of the electric double layer or EDL), we assume that the electrolyte solution can be represented by the primitive model, i.e., ions are charged hard spheres dispersed in a dielectric continuum.

The surface of the nanochannel is represented by a hard wall with the electrical potential fixed at $\Psi_0 = 0.5 \text{ V}$. The pressure gradient is also fixed at $2.17 \times 10^{13} \text{ Pa/m}$.

Our theoretical investigation is focused on the effect of ion size, valence, and different pairs of ionic species on the electrical current and the thermodynamic efficiency of the EKEC process as the height of the slit nanochannel varies from $h = 2$ to 7 nm . Approximately, the channel size is in the range consistent with recent experimental measurements.^{23, 24, 39} To calculate the thermodynamic efficiency, we need to evaluate the mechanical power for pushing the ionic fluid through the nanochannel, where L is the channel length, and Q stands for the volume flow rate. In terms of per unit width of the nanochannel, the flow rate can be calculated from an integration of the solvent velocity $v(y)$ inside the channel

$$Q = \int_0^h v(y) dy \quad (1)$$

As to be discussed in the following, we can determine the solvent velocity profile by solving the Navier-Stokes equation with the slip length obtained from MD simulation.

The electrical current per unit width of the nanochannel is related to both the local ion density $\rho_i(y)$ and the local ion velocity $v_i(y)$

$$I = e \int_0^h [\rho_+(y)v_+(y) - \rho_-(y)v_-(y)] dy, \quad (2)$$

where e is the elementary charge. Because there is no electrical field in the flow direction, the ion velocity is identical to the solvent velocity, $v(y) = v_+(y) = v_-(y)$.

The thermodynamic efficiency of the EKEC process, η , is defined as the ratio of the electrical power output W_e and the hydraulic power W_p . The electrical power can be expressed as

$$\eta = \frac{W_l}{W_p} = \frac{I^2 R}{W_p} \quad (3)$$

where R is the resistance. Therefore, we have

$$\eta \propto \frac{I^2}{W_p} \quad (4)$$

as the applicable standard for comparison of efficiency between different conditions. In practical applications, we are often interested in maximizing the thermodynamic efficiency at different conditions.

A. Calculation of the ionic distribution

As result of the ion size and electrostatic interactions, the ion distribution inside the nanochannel is not uniform. Conventionally, $\rho_i(y)$ is calculated from EDL models by assuming that the ion distribution satisfies local thermodynamic equilibrium. In most previous research, the EDL structure is determined by solving the Poisson-Boltzmann (PB) equation (or its modifications). In this work, the ionic density profiles are calculated from cDFT^{26, 40-42}

$$\rho_i(y) = \rho_i^b \exp\left[-\left(Z_i e \psi(y) + \Delta\mu_i^{ex}(y) + V_i^{ex}(y)\right) / (k_B T)\right], \quad (5)$$

where y is the perpendicular distance from the surface, $\psi(y)$ stands for the local electrical potential, ρ_i^b and Z_i represent the concentration and valence of the ionic specie i in the bulk, k_B and T are the Boltzmann constant and the absolute temperature, respectively. As in the PB equation, $\psi(y)$ can be solved from the Poisson equation with the boundary conditions

$$\psi(0) = \psi(h) = \Psi_0, \quad (6)$$

Eq. (6) means that the electrical potential at the channel surface is fixed.

In Eq. (5), $\Delta\mu_i^{ex}(y)$ is the deviation of the local excess chemical potential for species i from that corresponding to a uniform electrolyte solution with ionic density ρ_i^b , and $V_i^{ex}(y)$ represents the confining potential due to the slit wall. Within the primitive model of electrolyte solutions, each ion is represented by a hard sphere of diameter d_i , and $V_i^{ex}(y)$ in a slit pore of width h with hard walls is thus given by

$$V_i^{ex}(y) = \begin{cases} \infty, & y \leq d_i/2 \text{ or } y \geq h - d_i/2 \\ 0, & d_i/2 < y < h - d_i/2. \end{cases} \quad (7)$$

The theoretical details in cDFT calculations are reflected in terms of $\Delta\mu_i^{ex}(y)$ in Eq. (5). Within the primitive model, the thermodynamic non-ideality arises from electrostatic correlations and molecular excluded volume effects. The former is accounted for by a quadratic expansion of the excess Helmholtz energy with respect to that of a bulk system⁴³, and the latter is described by the modified fundamental measure theory (MFMT)⁴⁴. The explicit expression for μ_i^{ex} and numerical details for solving the cDFT equations can be found in our previous work⁴⁵.

B. Calculation of the slip length and velocity distribution

In the traditional study of hydrodynamics, the solvent velocity (v) along the vertical direction of the slit pore (y) is related to the pressure gradient ($\nabla p = \Delta p/l$) according to the Navier-Stokes (NS) equation

$$\eta_v \frac{d^2 v}{dy^2} - \nabla p = 0, \quad (8)$$

where η_v is the solvent viscosity. Although the viscosity near the interfacial layer is determined by the surface hydrophobicity⁴⁶, in this work, we follow the convention of the application of the Navier-Stokes equation⁴⁰ and the solvent viscosity is fixed at 0.89×10^{-3} Pa·s, corresponding to that of the bulk water at the ambient condition. We assume that solvent inhomogeneity near the

surface can be effectively described in terms of the slip length^{28, 47, 48}. By contrast, non-slip boundary conditions are often adopted in the traditional applications of the NS equation, i.e.,

$$v(0) = v(h) = 0. \quad (9)$$

The non-slip conditions are inconsistent with recent experimental results indicating large water flux inside nanochannels.^{34, 49, 50}

To estimate the slip length, we conducted a series of non-equilibrium MD simulations for the flow of water molecules inside graphene nanochannels with the pore width varying from 2 to 7 nm. A snapshot of the simulation box is shown in Fig. 1(b). The length and width of the channel are fixed at $l = 6.1$ nm and $h = 3.3$ nm, respectively. All MD simulations were implemented with the NAMD simulation package⁵¹. For each nanochannel, the surface consists of frozen carbon atoms, and the water molecules are represented by the SPC/E model.⁵² The SETTLE algorithm was used to maintain the rigid geometry of water molecules. A cut-off distance of 1.2 nm was applied to both the Lennard-Jones (LJ) potential and electrostatic interactions. The long-range correction of electrostatic interactions is computed via the particle mesh Ewald (PME) method. A leapfrog algorithm with a time step of 1.0 fs was used for time integration. At each condition, NPT simulations were carried out for 8 ns using the Nosé-Hoover Langevin piston and the dual Langevin thermostat with a damping coefficient of 5 ps to ensure that the system reaches the equilibration state at 300 K and 1 bar. At equilibrium, the average density of water molecules inside the pore was around 1.0 g/cm^3 . To calculate the slip length b , the NPT simulation was followed by non-equilibrium NVE simulation for 10 ns. Approximately, the average velocity of water molecules in the confined space obey the classical mechanics.^{53, 54} During the non-equilibrium simulation, the trajectories were collected every 0.5 ps, and an

additional fixed force was applied to oxygen atoms of the water molecules along the x axis as shown in Fig. 1 to mimic the pressure gradient effect on the water flow in the pore direction.

The slip length is closely related to the surface energy of the nanochannels. To study such effects, we conducted similar MD simulations the flow of water molecules in a slit pore. Following Radhakrishnan et al⁵⁵, we characterize the surface properties in terms of parameter α_w

$$\alpha_w = \rho_w \sigma_{aw}^2 \Delta_w \varepsilon_{aw} / \varepsilon_{aa} \quad (10)$$

where σ_{aw} and ε_{aw} are the LJ parameters for interaction between water and the surface, ε_{aa} is LJ parameters for SPC/E water, ρ_w is the number density of the surface atoms, and Δ_w is the separation between adjacent surface layers.

III. RESULTS AND DISCUSSION

A. Velocity profiles

As discussed above, non-equilibrium MD simulation allows us to determine the average velocity of water molecules in a slit pore driven by a pressure gradient. Fig. 2(a) shows typical simulation results and least-squares fitting to the NS equation by adjusting the slip length. For comparison, Fig.2(b) shows the prediction of the NS equation with the non-slip boundary conditions. Here the height of the nanochannel is 4 nm, and the wall properties is represented by the surface parameter $\alpha_w = 0.3$.

MD simulation indicates that the water velocity inside the slit pore is about 500 times larger than that predicted by the NS equation with the non-slip boundary conditions. The fast water flow in nanochannels is consistent with experiments^{32, 34, 56} and previous molecular simulations^{49, 57, 58}.

B. Effect of the surface properties on the slip length and electrical current

The slip length, and consequently the electrokinetic current, are closely related to the surface property parameter α_w and the nanochannel width h . Fig. 3 present the simulation results for the slip length. Here several MD simulation runs were conducted on the same conditions to obtain the mean and the error bars. Fig. 4 shows the electrical current per unit width predicted according to Eq. (2) with the ionic density calculated from cDFT and the solvent velocity profiles from the NS equation using the mean slip lengths from MD simulations.

As shown in Fig. 3, the slip length decreases with the increase of the surface parameters α_w , suggesting that the surface attraction reduces the slip length. Because the non-slip boundary condition corresponds to a vanishing solvent velocity at the surface, it is valid only when the attraction between the surface and water molecules is infinitely large. Such condition is not applicable to any realistic surfaces because of the limited surface attraction for water molecules. The non-slip boundary condition is particularly important for water flow through nanopores with the pore size comparable to the slip length. The simulation results explain why water flux detected in experiment is much larger than that predicted from the Navier-Stokes equation with the non-slip boundary condition.

Introducing the slip length into the NS equation results in a current density much larger than that from non-slip assumption. A comparison of the results shown in Fig. 5(a) and 5(b) indicates that the current density calculated with the slip lengths from MD simulation is almost 1,000 times larger than that without the slip length. This is consistent with the current density generated from the experiment results^{2, 19}. Because of the fast pressure-driven water flow, the electrical current cannot be described with the non-slip NS equation. As shown in Fig. 4, the current density declines with the increase of the surface parameter α_w due to the reduction in the

slip length and consequently the solvent velocity. The current density also decreases as the result of the reduction of the pore width because of the boundary effects.

C. Electrokinetic current and thermodynamic efficiency

A question of main practical interest is how the electrical current and thermodynamic efficiency depend on the solution conditions and the pore geometry and surface energy. To address this question, we applied the hybrid method described above to systems containing symmetric ion pairs (M^+N^- , $M^{2+}N^{2-}$) with of different concentrations, ranging from 1 mM to 1 M, and nanochannels with the pore width changing from 2 nm to 7 nm. All diameters of ions are 0.5 nm.

Fig. 5(a) and 5(b) show, respectively, the theoretical predictions of the current density for monovalent and divalent electrolytes at different concentrations. In both cases, the surface potential is 0.5 V, and the pressure gradient is fixed at 2.17×10^{13} Pa/m. The slipping lengths were obtained from cubic spline interpolation of MD results as shown in **Fig 3**. When the concentration increases from 1 mM to 1 M, the electrical current for monovalent system (M^+N^-) current increases. However, the trend is opposite for the divalent system ($M^{2+}N^{2-}$). In this case, the current density decreases as the ion concentration increases because of charge inversion.⁴⁰

As for the thermodynamic efficiency, the results from the non-slip Navier-Stokes equation indicate that the efficiency decreases when the height increases from 2 nm to 7 nm, but the results from Navier-Stokes equation with the slip length refute this inference as shown in **Fig. 6**. As shown in **Fig. 6**, the efficiency increases when the height increases from 2 nm to 5 nm, and reaches the maximum when the height is around 5 nm, then it decreases as the height increases to 7 nm. It is the result of the influence of the height on the slip length. As the increase of the height, the slip length increases, which results in the increase of water velocity inside the nanochannel

compared with that calculated from the traditional Navier-Stokes equations. The larger velocity increases the efficiency even when the height increases, and an optimal height can be derived to maximize the electrokinetic efficiency. Another different phenomenon from the traditional equations is that the efficiency of monovalent ions is larger than that of bivalent ions. Because of the precise description of water velocity inside the nanochannel from the modified equations, the influence of the net charge inversion found in bivalent ions on the electrokinetic efficiency is taken into account more accurately, which reduces the electrokinetic current and efficiency of the bivalent ions.

IV. CONCLUSIONS

In the present work, we predicted the current and thermodynamic efficiency of the slit nanochannels with different height and different concentrations of ions by the net charge profile from cDFT and velocity profile from MD simulation revised Navier-Stokes equation. Besides, we compared the results with that of non-slip Navier-Stokes equation to find out the effect of water behavior in the nanochannel on the current and efficiency. It is shown that the current of revised Navier-Stokes equation is about 1000 times larger than that of Navier-Stokes equation and with the same input hydraulic power. The phenomena mean that the non-ideality behavior of ions and water flow described by cDFT and the Navier-Stokes equation with the slip length, which is ignored by PB equation and Navier-Stokes equation, plays a significant role in the electrokinetic current and its thermodynamic efficiency. Surface properties are described by the parameter α_w , which indicates the interaction between surface atoms and water molecules. It shows that non-slip boundary condition is the extreme results of the attraction between the surface and water molecules. The relationship between the height and the efficiency is totally different from the results of the non-slip and the slip Navier-Stokes equation. Moreover, the

charge inversion phenomenon in multivalent ion flows reduces the current and efficiency, which refutes that in results of Navier-Stokes equation, the multivalent ion is better than monovalent for producing electrokinetic current. The above theoretical study with MD simulations provides a more precise method to describe the behavior of pressure-driven current in the nanochannels and new insights into this process. The results are helpful guidelines for design of pressure-driven devices and process.

Acknowledgement

This work is supported by the National Natural Science Foundation of China under grant No. U1862204 and No. 21878175. The numerical calculations were performed at the “Exploration 100” platform supported by Tsinghua National Laboratory for Information Science and Technology. JW acknowledges financial support by the Fluid Interface Reactions, Structures, and Transport (FIRST) Center, an Energy Frontier Research Center funded by the U.S. Department of Energy (DOE), Office of Science, Office of Basic Energy Sciences. This research used resources of the National Energy Research Scientific Computing Center, a DOE Office of Science User Facility supported by the Office of Science of the U.S. Department of Energy, under Contract DE-AC02-05CH11231.

Reference

1. F. A. Morrison and J. F. Osterle, *J Chem Phys*, 1965, **43**, 2111-&.
2. A. Siria, P. Poncharal, A. L. Biance, R. Fulcrand, X. Blase, S. T. Purcell and L. Bocquet, *Nature*, 2013, **494**, 455-458.
3. F. H. J. van der Heyden, D. Stein and C. Dekker, *Phys Rev Lett*, 2005, **95**.
4. P. H. Yang, X. P. Qu, K. Liu, J. J. Duan, J. Li, Q. Chen, G. B. Xue, W. K. Xie, Z. M. Xu and J. Zhou, *Acs Appl Mater Inter*, 2018, **10**, 8010-8015.
5. L. J. Mei, L. H. Yeh and S. Z. Qian, *Nano Energy*, 2017, **32**, 374-381.
6. D. K. Kim, D. Kim, S. J. Kim and S. J. Park, *Int J Therm Sci*, 2010, **49**, 1128-1132.
7. Y. B. Liu and Y. J. Jian, *Acta Phys Sin-Ch Ed*, 2016, **65**.
8. Y. J. Jian, F. Q. Li, Y. B. Liu, L. Chang, Q. S. Liu and L. G. Yang, *Colloid Surface B*, 2017, **156**, 405-413.
9. C. L. A. Berli, *J Colloid Interf Sci*, 2010, **349**, 446-448.

10. H. F. Cheng, Y. Zhou, Y. P. Feng, W. X. Geng, Q. F. Liu, W. Guo and L. Jiang, *Adv Mater*, 2017, **29**.
11. C. Davidson and X. C. Xuan, *J Power Sources*, 2008, **179**, 297-300.
12. Y. Zhang, Y. H. He, M. Tsutsui, X. S. Miao and M. Taniguchi, *Sci Rep-Uk*, 2017, **7**.
13. Y. Q. Ren and D. Stein, *Nanotechnology*, 2008, **19**.
14. X. C. Xuan and D. Q. Li, *J Power Sources*, 2006, **156**, 677-684.
15. D. Burgreen and F. R. Nakache, *J Appl Mech*, 1965, **32**, 675-&.
16. D. Gillespie, *Nano Lett*, 2012, **12**, 1410-1416.
17. A. Mansouri, S. Bhattacharjee and L. Kostiuk, *Lab Chip*, 2012, **12**, 4033-4036.
18. W. Olthuis, B. Schippers, J. Eijkel and A. van den Berg, *Sensor Actuat B-Chem*, 2005, **111**, 385-389.
19. S. Haldrup, J. Catalano, M. Hinge, G. V. Jensen, J. S. Pedersen and A. Bentien, *Acs Nano*, 2016, **10**, 2415-2423.
20. S. Haldrup, J. Catalano, M. R. Hansen, M. Wagner, G. V. Jensen, J. S. Pedersen and A. Bentien, *Nano Lett*, 2015, **15**, 1158-1165.
21. Y. B. Xie, D. Bos, L. J. de Vreede, H. L. de Boer, M. J. van der Meulen, M. Versluis, A. J. Sprenkels, A. van den Berg and J. C. T. Eijkel, *Nat Commun*, 2014, **5**.
22. D. M. Rowe, *Thermoelectrics handbook: macro to nano*, CRC press, 2018.
23. B. S. Kilsgaard, S. Haldrup, J. Catalano and A. Bentien, *J Power Sources*, 2014, **247**, 235-242.
24. J. Catalano and A. Bentien, *J Power Sources*, 2014, **262**, 192-200.
25. Y. Yan, Q. Sheng, C. M. Wang, J. M. Xue and H. C. Chang, *J Phys Chem C*, 2013, **117**, 8050-8061.
26. X. Kong, J. Jiang, D. N. Lu, Z. Liu and J. Z. Wu, *J Phys Chem Lett*, 2014, **5**, 3015-3020.
27. M. Whitby and N. Quirke, *Nat Nanotechnol*, 2007, **2**, 87-94.
28. H. B. Huang, Z. G. Song, N. Wei, L. Shi, Y. Y. Mao, Y. L. Ying, L. W. Sun, Z. P. Xu and X. S. Peng, *Nat Commun*, 2013, **4**.
29. R. R. Nair, H. A. Wu, P. N. Jayaram, I. V. Grigorieva and A. K. Geim, *Science*, 2012, **335**, 442-444.
30. H. W. Dai, Z. J. Xu and X. N. Yang, *J Phys Chem C*, 2016, **120**, 22585-22596.
31. G. Hummer, J. C. Rasaiah and J. P. Noworyta, *Nature*, 2001, **414**, 188-190.
32. M. Majumder, N. Chopra, R. Andrews and B. J. Hinds, *Nature*, 2005, **438**, 44.
33. M. Whitby, L. Cagnon, M. Thanou and N. Quirke, *Nano Lett*, 2008, **8**, 2632-2637.
34. J. K. Holt, H. G. Park, Y. M. Wang, M. Stadermann, A. B. Artyukhin, C. P. Grigoropoulos, A. Noy and O. Bakajin, *Science*, 2006, **312**, 1034-1037.
35. Y. L. Zhu, K. Zhan and X. Hou, *Acs Nano*, 2018, **12**, 908-911.
36. J. C. T. Eijkel and A. van den Berg, *Microfluid Nanofluid*, 2005, **1**, 249-267.
37. A. K. Rasheed, M. Khalid, W. Rashmi, T. C. S. M. Gupta and A. Chan, *Renew Sust Energ Rev*, 2016, **63**, 346-362.
38. D. G. Haywood, A. Saha-Shah, L. A. Baker and S. C. Jacobson, *Anal Chem*, 2015, **87**, 172-187.
39. C. Duan and A. Majumdar, *Nat Nanotechnol*, 2010, **5**, 848.
40. X. Y. Hu, X. Kong, D. N. Lu and J. Z. Wu, *J Chem Phys*, 2018, **148**.
41. X. Kong, A. Gallegos, D. Lu, Z. Liu and J. Wu, *Physical Chemistry Chemical Physics*, 2015, **17**, 23970-23976.
42. X. Kong, J. Wu and D. Henderson, *J Colloid Interf Sci*, 2015, **449**, 130-135.

43. Z. D. Li and J. Z. Wu, *Phys Rev E*, 2004, **70**.
44. Y. X. Yu and J. Z. Wu, *J Chem Phys*, 2002, **117**, 10156-10164.
45. J. Z. Wu, T. Jiang, D. E. Jiang, Z. H. Jin and D. Henderson, *Soft Matter*, 2011, **7**, 11222-11231.
46. S. Majumder, J. Dhar and S. Chakraborty, *Sci Rep-Uk*, 2015, **5**, 14725.
47. N. R. Tas, J. Haneveld, H. V. Jansen, M. Elwenspoek and A. van den Berg, *Appl Phys Lett*, 2004, **85**, 3274-3276.
48. R. Qiao and N. R. Aluru, *Appl Phys Lett*, 2005, **86**.
49. S. K. Kannam, B. Todd, J. S. Hansen and P. J. Davis, *The Journal of chemical physics*, 2013, **138**, 094701.
50. J. A. Thomas and A. J. McGaughey, *Nano Lett*, 2008, **8**, 2788-2793.
51. J. C. Phillips, R. Braun, W. Wang, J. Gumbart, E. Tajkhorshid, E. Villa, C. Chipot, R. D. Skeel, L. Kale and K. Schulten, *J Comput Chem*, 2005, **26**, 1781-1802.
52. H. Berendsen, J. Grigera and T. Straatsma, *Journal of Physical Chemistry*, 1987, **91**, 6269-6271.
53. S. Bernardi, B. D. Todd and D. J. Searles, *J Chem Phys*, 2010, **132**.
54. M. Ma, F. Grey, L. M. Shen, M. Urbakh, S. Wu, J. Z. Liu, Y. L. Liu and Q. S. Zheng, *Nat Nanotechnol*, 2015, **10**, 692-695.
55. R. Radhakrishnan, K. E. Gubbins and M. Sliwinska-Bartkowiak, *The Journal of Chemical Physics*, 2000, **112**, 11048-11057.
56. M. Majumder and B. Corry, *Chemical Communications*, 2011, **47**, 7683-7685.
57. M. D. Ma, L. Shen, J. Sheridan, J. Z. Liu, C. Chen and Q. Zheng, *Phys Rev E*, 2011, **83**, 036316.
58. K. Falk, F. Sedlmeier, L. Joly, R. R. Netz and L. Bocquet, *Nano Lett*, 2010, **10**, 4067-4073.

Figure Captions

Figure 1. Schematic illustration of the model. (a) Ions in the slit nanochannel of height h and length l . (b) Non-equilibrium MD simulation structure of the unit cell drawn by VMD.

Graphite is cyan and fixed and water molecules are inside the nanochannel. The height of the nanochannel here is 1 nm. Additional force was applied on the water to simulate the pressure difference.

Figure 2. Velocity distribution from MD simulation and non-slipping Navier-Stokes Equation. The height of the channel is 4 nm. (a) Velocity distribution along y -axis from MD simulation and its quadric fitting to derive slipping length b . (b) Velocity distribution from non-slipping Navier-Stokes equation.

Figure 3. Relation between slipping length b and a_w for different heights of the channel. The solid lines are guides to the eye indicating trends in b as functions of a_w

Figure 4. Relation between current per height (I/h) and a_w for different heights of the channel.

Figure 5. Electrokinetic current in height-different nanochannels with velocity calculated by Navier-Stokes Equation (inset) or MD simulations. (a) $Z_i=1$; (b) $Z_i=2$;

The gradient of the pressure is fixed at 2.17×10^{13} Pa/m in velocity calculation for MD sampling and the potential of the nanochannel is fixed at 0.5 V for calculation of ion concentration distribution.

Figure 6. Efficiency of energy conversion in height-different nanochannels with velocity calculated by Navier-Stokes Equation (inset) or MD simulations. (a) $Z_i=1$; (b) $Z_i=2$;

Figure 1

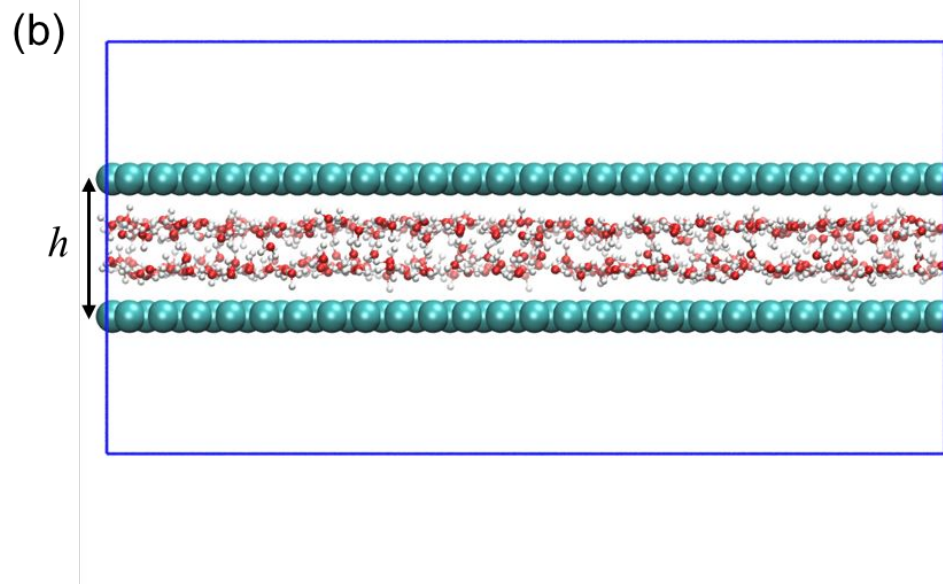
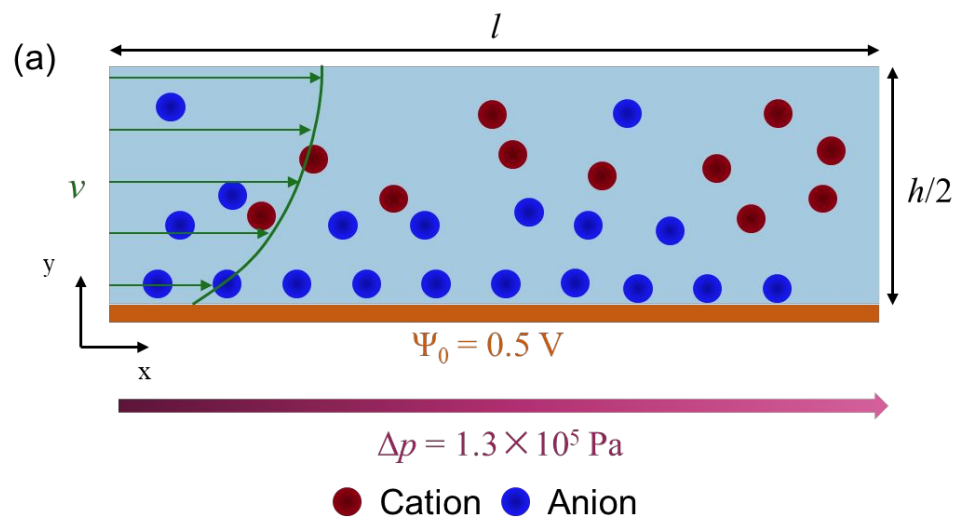


Figure 2

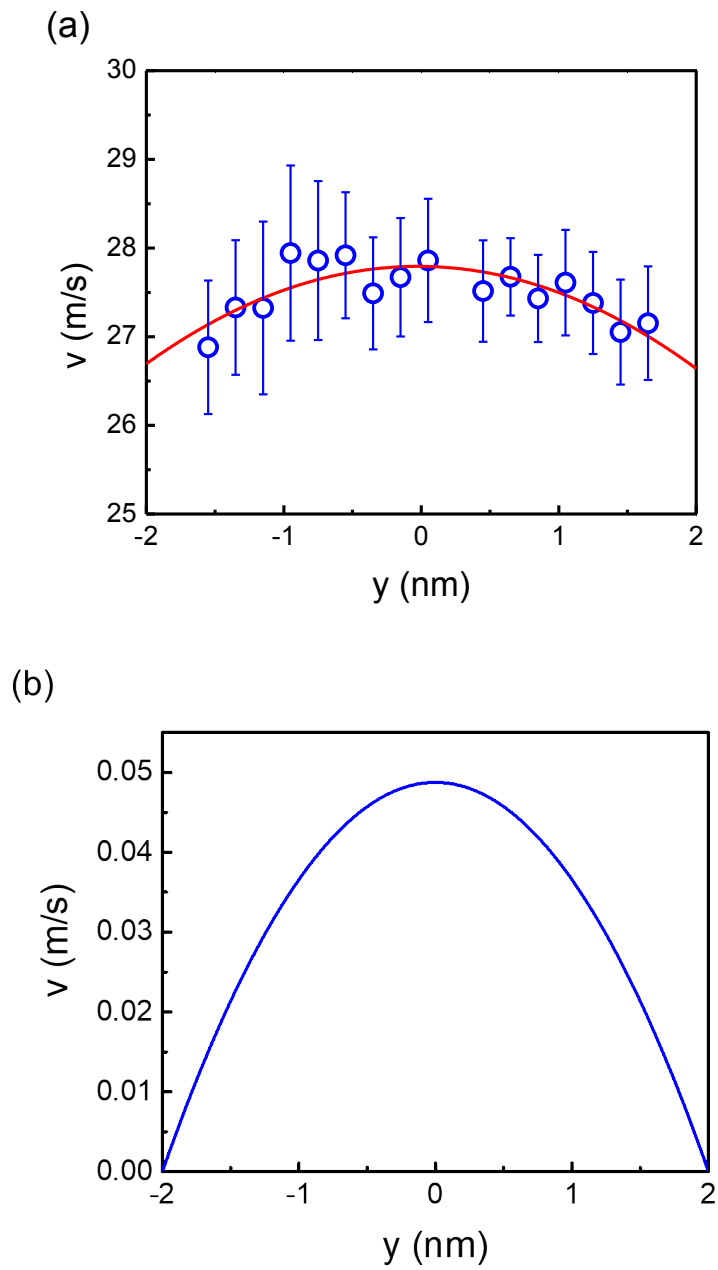


Figure 3

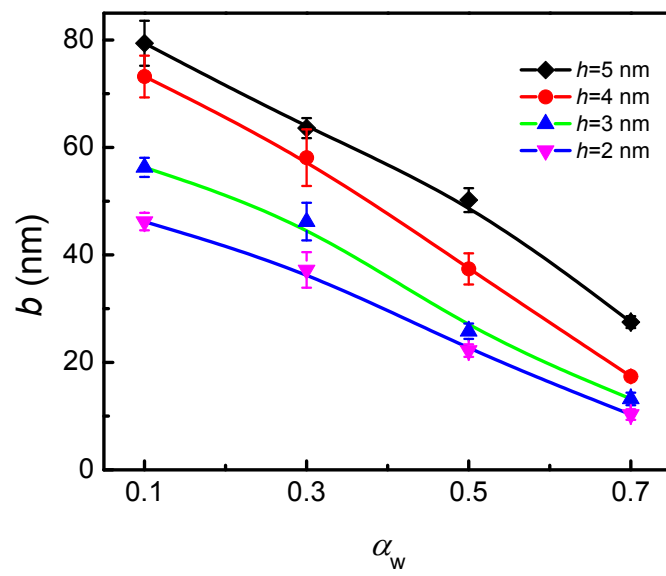


Figure 4

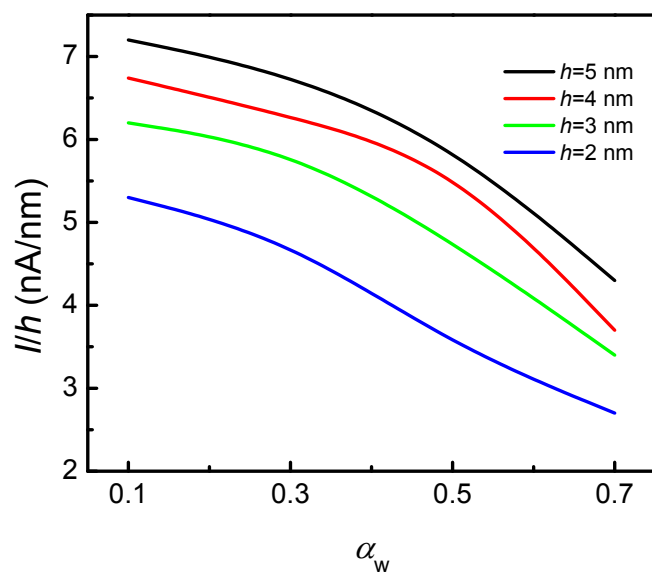


Figure 5

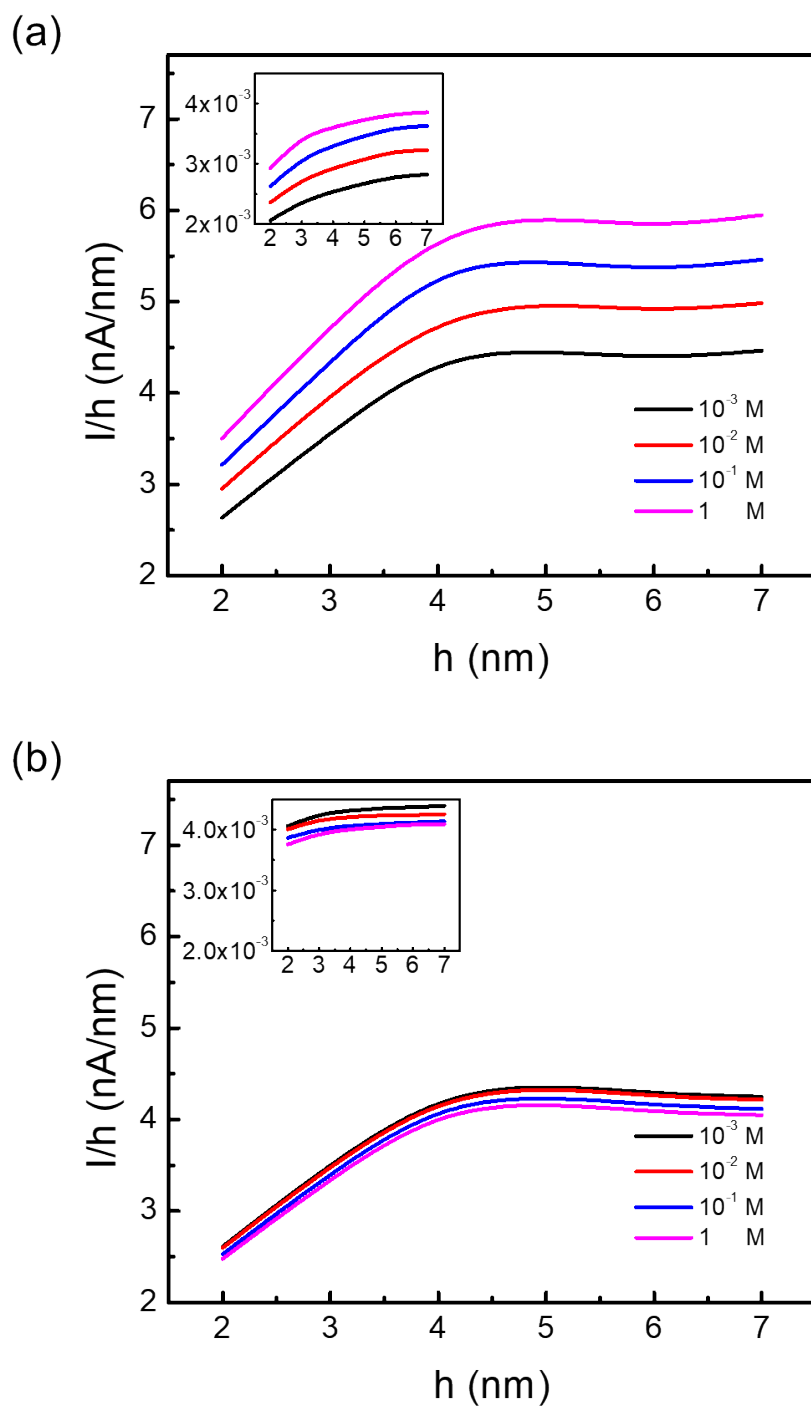


Figure 6

